RESEARCH ARTICLE

Check for updates

Effectively designing infrared nonlinear optical materials with magnetism, MMn₆Ga₆S₁₆ (M = Ca, Sr, Ba, and Pb), aided by stable open frameworks†

Kaixuan Li, Yujie Zhang, Xianchao Zhu, [iD] * Hongping Wu, [iD] * Zhanggui Hu, Jiyang Wang and Yicheng Wu

Infrared nonlinear optical (NLO) materials are crucial to the development of laser technology. However, finding ways to effectively synthesize them is still a big challenge. Herein, aided by a stable open framework, four IR NLO materials, $MMn_6Ga_6S_{16}$ (M = Ca, Sr, Ba, and Pb), have been effectively synthesized in a high-temperature vacuum sealing system. They all crystallize in a non-centrosymmetric (NCS) space group, $P\bar{6}$, and their structures feature a three-dimensional open framework composed of Mn–S single and double chains and Ga–S single and double chains, in which these one-dimensional chains increase the structural flexibility and adjustability to accommodate varied cations with different ionic radii. Remarkably, $MMn_6Ga_6S_{16}$ (M = Ca, Sr, Ba, and Pb) exhibit not only comprehensive NLO performances including appropriate NLO responses and band gaps and a wide transmission range but also *para*-magnetism in magnetic properties, indicating that $MMn_6Ga_6S_{16}$ (M = Ca, Sr, Ba, and Pb) are potential IR multifunctional materials. This work suggests that a stable open framework can be used to construct varied structures, which brings a new platform for effectively designing multifunctional materials.

Introduction

Infrared (IR) coherent lights, covering two important atmospheric windows (3–5 and 8–12 μm), have important applications in laser guidance and radar, atmospheric detection, and infrared remote sensing. Utilizing the frequency conversion of nonlinear optical (NLO) crystals is an effective way to generate coherent radiation over a range of different wavelengths.[1–6] Presently, a large number of nonlinear optical materials have been discovered and synthesized, including oxides and chalcogenides,[7–12] but in reality, the insufficient optical transparency and low second-harmonic generation (SHG) response of oxides are not suitable for their application in the IR region. Chalcogenides have been considered the preferred candidates to explore IR materials due to their unique structures composed of typical tetrahedral NLO-active genes, *i.e.* the main-group metal elements (*e.g.*, Ga, In, Si, Ge, and Sn) coordinated with chalcogen atoms to form asymmetric configurations.[13–17] These structural advantages are favorable for large SHG coefficients and a wide optical transparency

window up to the IR region, such as those of commercialized chalcopyrite-type $AgGaQ_2$ (Q = S, Se) and $ZnGeP_2$.[18–20] However, own performance defects hinder their application ranges, and with this background, effectively designing and synthesizing IR NLO materials have become the important task for researchers.

In crystal engineering, taking classical structures as templates or evolving these structures is an efficient way to explore new IR NLO materials in chalcogenides.[21–24] For example, based on the type of melilite structure, a number of chalcogenides, *i.e.* $Sr_2ZnSn_2OS_6$,[25] $Ca_2GeGa_2OS_6$ [26] and $Sr_2MnGe_2OS_6$,[27] have been developed. $Sr_2ZnSn_2OS_6$ shows excellent NLO properties including a high SHG (0.7 × AGS), a wide optical band gap (E_g = 3.52 eV), and suitable birefringence (Δn = 0.14@2090 nm). Besides, by assembling different host and guest functional units in salt inclusion chalcogenides (SICs), many new compounds can be designed and synthesized with diverse structures and unique properties,[28] such as the nano-tunnel type $[K_3Cl][Mn_2Ga_6S_{12}]$ and $[Cs_6Cl][Ga_5GeQ_{12}]$ (Q = S, Se) in the $[R_aX_b][M_cQ_d]$ family (R = alkali or alkali-earth metals; X = halogen; M = main-group or transition metals; and Q = chalcogen) and $[NaSr_4Cl][Ge_3S_{10}]$ with isolated $[Ge_3S_9]$ rings and one-dimensional $[ClNaSr_3]_\infty^{6+}$ chains.[29–31] Based on the above analysis, it is not hard to notice that the selection of a suitable framework is conducive to designing new NLO materials.[32]

After extensive screening and in-depth analysis, we noticed that the A(ɪ)B₃C₃Q₈ (A = Ag, Li, Na, Cu; B = Mg; C = Al, Ga; Q =

Tianjin Key Laboratory of Functional Crystal Materials, Institute of Functional Crystal, Tianjin University of Technology, Tianjin 300384, China

This journal is © the Partner Organisations 2024

Inorg. Chem. Front., 2024, **11**, 5465–5472 | **5465**

S, Se) family exhibits excellent linear or nonlinear performances, and in the structures,[33] the A-, B-, and C-sites can be replaced by various cations with different electronic configurations, in which, the framework is still stable, suggesting that it may be a good template to design NLO materials combined with the chemical substitution method. In this series of compounds, alkali metal $AMg_3Ga_3S_8$ (A = Li, Na) and AE(II) $Mg_6Ga_6Q_{16}$ (AE = Ca, Sr, Ba, Q = S, Se) with two types of alkaline earth metals have been reported, and among them, the optical band gaps of $LiMg_3Ga_3S_8$ and $NaMg_3Ga_3S_8$ are up to 3.86 and 3.70 eV, respectively, but their second harmonic coefficients are relatively small. However, under the action of 'the two types of alkaline earth metals' or 'rare earth metals and alkaline earth metals', $AEMg_6Ga_6S_{16}$ (AE = Ca, Sr, Ba) and $LaMg_6Ga_6S_{16}$ not only have large second harmonic effects (≈0.7–0.8 × AGS), but also possess wide optical band gaps (E_g = 3.00–3.54 eV).[34–36] It can be seen that in the family of A(I) $B_3C_3Q_8$, the A-site cations have a significant effect on their performances. To date, the element substitution of A- and C-sites has led to the formation of many new compounds and the substitution effects on the structure and performances have been investigated, whereas there are no direct studies on the B-sites, as an important component of the structural framework, to determine their effect on the stability of structures and properties. Not long ago, our group had successfully synthesized $NaMn_3Ga_3S_8$.[37] In this work, we will continue to change the B-site of the $AEMg_6Ga_6S_{16}$ (AE = alkaline earth metals) family by introducing Mn^{2+} cations and further study the effects of chemical substitution on its structure and properties. Four new non-centrosymmetric (NCS) chalcogenides $MMn_6Ga_6S_{16}$ (M = Ca, Sr, Ba, Pb) have been successfully synthesized. Structurally, all these compounds crystallize in the NCS hexagonal space group $P\bar{6}$ and contain Mn–S and Ga–S single and double chains, which provide the flexibility for the formation of open frameworks to match different A-site cations. Property measurements show that $MMn_6Ga_6S_{16}$ (M = Ca, Sr, Ba, Pb) not only exhibit NLO performances but also possess magnetic properties compared with the Ga-based family.[38] Besides, a detailed structural comparison has been carried out in A(I) $B_3C_3Q_8$ and $AE(II)Mg_6Ga_6Q_{16}$ to elaborate on the designability of the structure.

Results and discussion

Crystal structures

The structures of $CaMn_6Ga_6S_{16}$ (CMGS), $SrMn_6Ga_6S_{16}$ (SMGS), $BaMn_6Ga_6S_{16}$ (BMGS), and $PbMn_6Ga_6S_{16}$ (PMGS) were determined by single-crystal XRD. The results showed that they were isostructural and crystallized in the NCS hexagonal space group $P\bar{6}$ (Table S1, ESI†). Taking CMGS as an example, its asymmetric unit contains 3 unique Ca atoms, 6 unique Mn atoms, 3 unique Ga atoms, and 11 S atoms (Table S2†). The Mn atom is linked with six S atoms to form a MnS_6 octahedron, with Mn–S distances of 2.524(3)–2.769(4) Å. Furthermore, the MnS_6 octahedra are connected with each

other to construct one-dimensional (1D) Mn–S single and double chains (Fig. 1a). The Mn–S single chains are linked with Mn–S double chains to form 1D tunnels along the c-axis (Fig. 1b). Also, the Ga atoms are coordinated with four S atoms to form GaS_4 tetrahedra (Fig. 1c), and their combination subsequently results in the formation of Ga–S single and double chains with Ga–S distances ranging from 2.221(3)–2.322(2) Å. Then, Ga–S double chains are linked with 1D tunnels composed of MnS_6 to construct an open framework, in which the GaS_4 single chains and Ca^{2+} cations are located in the space (Fig. 1d). The values for the bond valence sum (BVS) for each atom are in the range of 1.57–1.60 for Ca, 1.78–1.84 for Sr, 2.11–2.21 for Ba, 1.59–1.68 for Pb, 2.93–2.97 for Ga, 1.90–1.98 for Mn and 1.82–2.12 for S (Table S2†).[39] These are all consistent with the expected oxidation states. By comparing the structures of CMGS, SMGS, BMGS, and PMGS, it was found that the open $[Mn/Ga–S]_\infty$ framework can be filled by cations of different sizes (Ca: 197 pm, Sr: 215 pm, Ba: 222 pm, and Pb: 175 pm), indicating that their structural framework is stable and flexible.

Structural comparison

In the systems of $A(I)B_3C_3Q_8$ (A = alkali metal) and AE(II) $Mg_6Ga_6Q_{16}$ (AE = alkaline-earth metal), there are 21 compounds containing the title compounds $MMn_6Ga_6S_{16}$ (M = Ca, Sr, Ba, and Pb). They all crystallize in the same NCS space group of $P\bar{6}$. They also contain a similar structural framework. These compounds all can be seen as the derivative of A(I) $B_3C_3Q_8$. Owing to the similarity of these structures, their lattice constants are also related. For $A(I)B_3C_3Q_8$ to AE(II) $Mg_6Ga_6Q_{16}$, a = $b_{(A)}$ ≈ a = $b_{(AE)}$, while the length of the crystallographic c-axis of $AE(II)Mg_6Ga_6Q_{16}$ is almost two times that of $A(I)B_3C_3Q_8$ due to the substitution of the alkali metal by the alkaline-earth metal. This substitution results in the ordered vacancies forming at the A site in $MMn_6Ga_6S_{16}$ (M = Ca, Sr) or partially occupied by the Ba or Pb atoms in $M'Mn_6Ga_6S_{16}$ (M' = Ba, Pb) (Fig. S6†). As for B and C site substitution, the lattice constants hardly changed in $AE(II)Mg_6Ga_6Q_{16}$ (Table S3†). Structurally, all structures contain an open framework composed of a series of B- and C-based chains. These chains provide the flexibility and adjustability for scaling up and down of channels in the structures that can accommodate different A-site cations. For example, as the radius increases from Li to Na in $AMg_3Ga_3S_8$ (Fig. 2a and b), the radii of the tunnels composed of the Mg- and Ga-based chains also increase (Fig. 2g). However, when A = Ag, the coordination environment changes from six-fold coordinated LiS_6 or NaS_6 to three-coordinated AgS_3, and the location of A-site cations also changes, i.e. in $LiMg_3Ga_3S_8$ and $NaMg_3Ga_3S_8$, the Li and Na atoms are nearly coplanar with Mg atoms, while the Ag atoms are coplanar with Ga atoms in $AgMg_3Ga_3S_8$ (Fig. 2f). Besides, at A-sites, the alkali metals were replaced by the alkaline earth metals, and accordingly, the radius of the tunnels also increases (Table S6†). This analysis indicates that the sites of filled cations can self-adjust with the difference in their radii and coordination environment, further presenting the flexi

5466 | *Inorg. Chem. Front.*, 2024, **11**, 5465–5472

This journal is © the Partner Organisations 2024
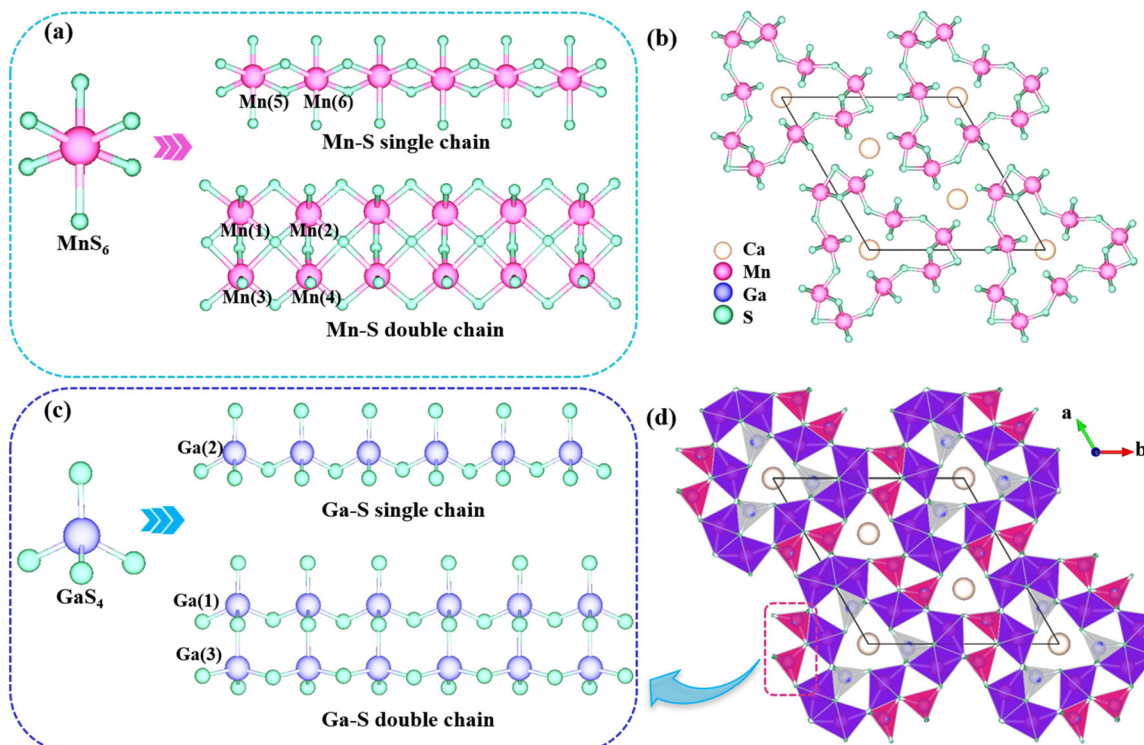
Fig. 1 Crystal structure of CMGS: (a) MnS_6 octahedron and Mn−S single and double chains; (b) Mn_9S_{39} framework; (c) GaS_4 tetrahedron and Ga−S single and double chains; and (d) structure of CMGS viewed along the c-axis.
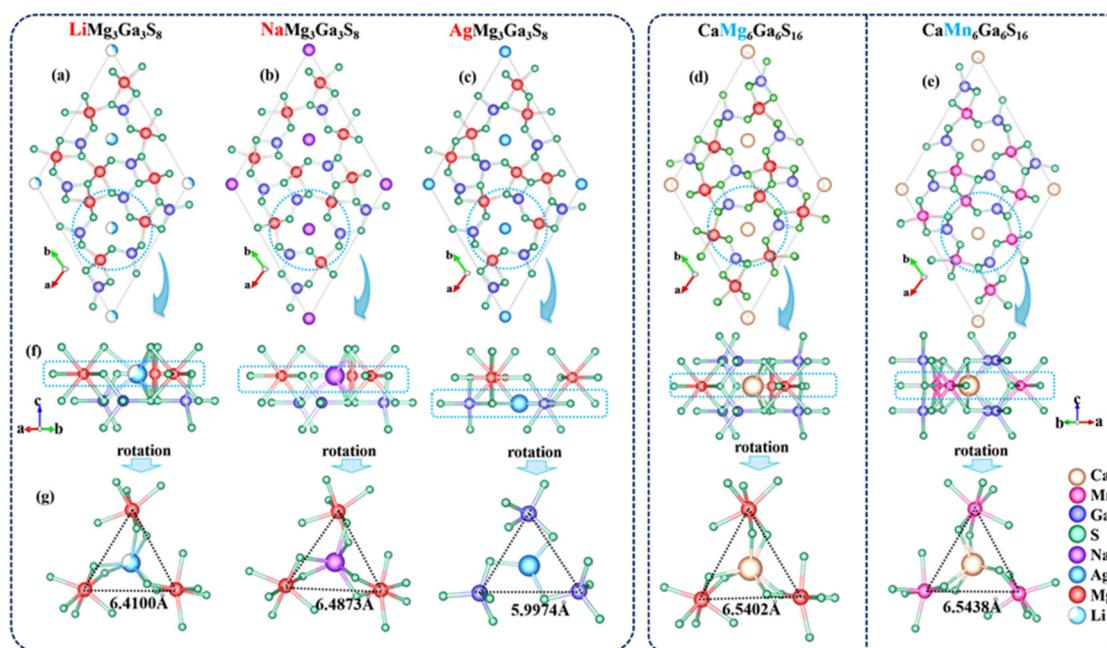
Fig. 2 Structures of (a) $LiMg_3Ga_3S_8$; (b) $NaMg_3Ga_3S_8$; (c) $AgMg_3Ga_3S_8$; (d) $CaMg_6Ga_6S_{16}$; and (e) $CaMn_6Ga_6S_{16}$; and (f and g) the location of different cations.

bility of these constituted chains. However, to date, there is no related report about the B-site substitution in $AE(II)Mg_6Ga_6Q_{16}$. So, the title compounds, $MMn_6Ga_6S_{16}$ (M = Ca, Sr, Ba, Pb), represent the first example of B-site change based on the structure of $AE(II)Mg_6Ga_6Q_{16}$. It is worth noting that the B-site substitution results in some structural difference; for example, when

This journal is © the Partner Organisations 2024

Inorg. Chem. Front., 2024, **11**, 5465–5472 | **5467**

Mg^{2+} ions were successfully replaced by Mn^{2+} ions, the radii of the channels increased, suggesting that the atomic radius of the Mn ion as an important component of the channels directly affects the size of the channels' radii. Based on the above analysis, we can conclude that the varied chain structure may provide the flexibility to build the open framework to accommodate different cations, which is favorable for the design of new compounds.

Optical properties

The polycrystalline samples were synthesized using a high-temperature solid-state reaction in a closed vacuum environment, and the purity was checked by powder X-ray diffraction (Fig. S1†). The Rietveld refinement of the powder XRD profile for CMGS is shown in Fig. 3a. The R value of $R_P = 0.08$ indicates that the fitted profile matches the experimental data well. Then, the polycrystalline samples were used for the performance characterization. The UV-vis-NIR diffuse reflectance spectra for these compounds are shown in Fig. S2.† Converting the diffuse reflectance spectra to absorption by the Kubelka–Munk equation is shown in Fig. 3b. It is clear that the experimental band gaps of the title compounds were 2.58 eV (CMGS), 2.40 eV (SMGS), 2.55 eV (BMGS), and 2.05 eV (PMGS), which are consistent with their crystal colors (their crystal colors are cyan, light green, green, and orange, respectively). In addition, the laser induced damage threshold (LIDT) was determined using the single-pulse measurement method, and the values were 40.5, 45.4, 47.7 and 41.3 MW cm^{-2} for $MMn_6Ga_6S_{16}$ (M = Ca, Sr, Ba, Pb) with the particle size ranging from 180–250 μm, respectively, which were higher than that of AGS (8.5 MW cm^{-2}) under the same conditions.[40] These results indicated that $MMn_6Ga_6S_{16}$ (M = Ca, Sr, Ba, Pb) can withstand higher power laser irradiation. The IR spectra are shown in Fig. 3c. It was found that these title compounds have a wide infrared transmission range from 600 to 4000 cm^{-1} that covers the two atmospheric windows (3–5 and 8–12 μm) for the important applications in telecommunications, laser guidance, and explosive detection.

Besides, the birefringence of the crystals of $MMn_6Ga_6S_{16}$ (M = Ca, Sr, Ba, Pb) has been measured by using a cross-polarization microscope based on the formula $R = \Delta n \times d$, where R, Δn, and d represent the optical path difference, birefringence, and thickness, respectively.[41,42] The original interference color is shown in Fig. 3d–f (Fig. S3†). The crystal thickness was measured by using a single crystal diffractometer, and the thicknesses were 26.6 μm (CMGS), 28.8 μm (SMGS), 19.9 μm (BMGS) and 28.3 μm (PMGS). The optical path differences were obtained to be 1200, 1300, 1300 and 1400 nm for CMGS, SMGS, BMGS and PMGS, respectively, by comparing with the Michel-Lévy chart. Then, the birefringence values were determined to be 0.045 (CMGS), 0.046 (SMGS), 0.060 (BMGS) and 0.049 (PMGS) in the visible region. The suitable birefringence is favorable to achieve a wide phase matching (PM) region.[43]

These title compounds are all NCS structures, which is an essential prerequisite for an NLO response. So, the SHG intensity *versus* the particle sizes of $MMn_6Ga_6S_{16}$ (M = Ca, Sr, Ba, Pb) has been investigated based on the Kurtz–Perry method with a Q-switched Ho : Tm : Cr : YAG laser (2.09 μm, 3 Hz, 50 ns).[44] As shown in Fig. 4a, the SHG intensities increase with the particle size increasing in the range of 30–210 μm, indicating that $MMn_6Ga_6S_{16}$ are phase-matchable and the SHG intensities of these compounds are 0.4–0.7 times that of AGS with
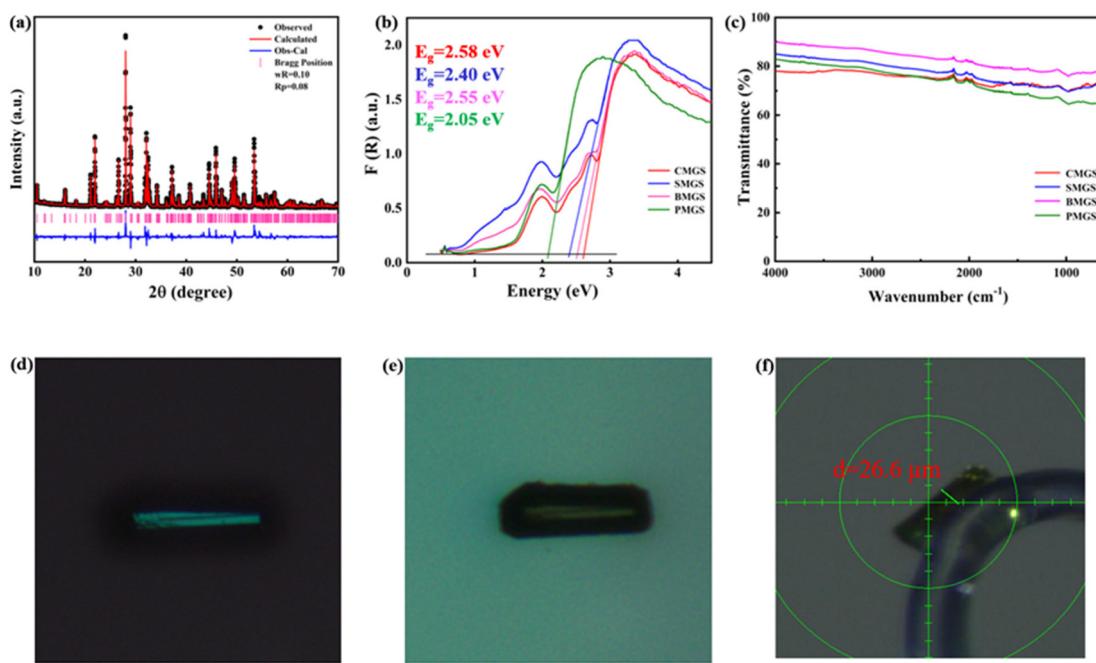
Fig. 3 (a) Rietveld refinement of the powder XRD profile for CMGS; (b) band gaps of $MMn_6Ga_6S_{16}$ (M = Ca, Sr, Ba, and Pb); (c) IR spectra of $MMn_6Ga_6S_{16}$ (M = Ca, Sr, Ba, and Pb); and (d−f) the original interference color, extinction, and thickness of the CMGS crystal, respectively.

5468 | *Inorg. Chem. Front.*, 2024, **11**, 5465–5472

This journal is © the Partner Organisations 2024
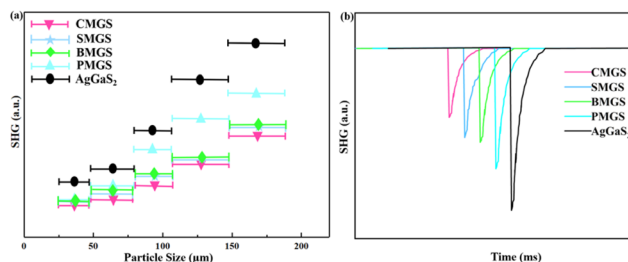
Fig. 4 (a) Phase-matching results of $MMn_6Ga_6S_{16}$ (M = Ca, Sr, Ba, and Pb) and the benchmark AGS at 2090 nm and (b) SHG intensities of $MMn_6Ga_6S_{16}$ (M = Ca, Sr, Ba, and Pb) and AGS with the particle size ranging from 150–200 μm.

the particle size ranging from 150–210 μm. For PMGS, its SHG strength is up to 0.7 times that of AGS (Fig. 4b), greatly improving the NLO response compared with $A(I)B_3C_3S_8$ (Table S3b†). To further investigate the NLO properties, we further analyzed the distortion (Δd) of MnS_6 or MgS_6 and GaS_4 in $MMn_6Ga_6S_{16}$ (M = Ca, Sr, Ba, Pb), $La_6MnGe_2S_{14}$, La_3MnGaS_7,[45] $LiGaS_2$,[46] α-$BaGa_4S_7$[47] and $AeMg_6Ga_6S_{16}$ (Ae = Ca, Sr, Ba). The calculated results show that the distortion of the MnS_6 octahedron is larger than that in $La_6MnGe_2S_{14}$ and La_3MnGaS_7, while the GaS_4 tetrahedron exhibits similar distortion to that in α-$BaGa_4S_7$ and $AeMg_6Ga_6S_{16}$ (Ae = Ca, Sr, Ba) (Tables S5a and b†). These indicate that the distorted MnS_6 and GaS_4 and their regular arrangement are conducive to the SHG response (Fig. S4†).

Magnetic properties

The title compounds all contain the Mn^{2+} ions, which may make these compounds exhibit magnetic properties. As such, the dependence of magnetization (M–T) of polycrystalline powder was tested in the temperature range of 3–300 K (zero field cooling (ZFC) and field cooling (FC)) with an applied electric field of $H = 5000$ Oe.[48,49] The molar magnetic susceptibility (χ) and the inverse molar magnetic susceptibility (χ^{-1}) as a function of temperature (T K^{-1}) are shown in Fig. S5.† The magnetic susceptibility decreases gradually with the increase in temperature, which is a typical characteristic of a paramagnetic compound conforming to the Curie–Weiss law. In addition, according to the Curie–Weiss law, by extrapolating the high-temperature paramagnetic curve of χ^{-1}–T as a straight line, we can obtain the intercept on the T-axis, which is the Curie–Weiss temperature (T_W) and the slope is $1/C$ (C is the Curie constant).[50,51] The fitted Curie constant (C) and Weiss temperature (T_W) are 4.73 emu K mol^{-1} and −130.71 K for CMGS, respectively. Similar results were obtained for compounds $SrMn_6Ga_6S_{16}$, $BaMn_6Ga_6S_{16}$ and $PbMn_6Ga_6S_{16}$ (Table S3a†). The negative T_W values suggest weak short-range antiferromagnetic interactions among the adjacent magnetic cations. Then, according to the $\mu_{eff} = (8C)^{1/2}\mu_B$ equation, the experimental effective magnetic moment (μ_{eff}) of Mn(II) in CMGS is $6.15\mu_B$, which is consistent with the theoretical one of Mn(II) ($5.92\mu_B$).[52]

Furthermore, we noted that CMGS has a similar structure to that of $NaMn_3Ga_3S_8$ previously reported by our group;

however, $NaMn_3Ga_3S_8$ exhibits antiferromagnetic behavior.[37] Structural analysis shows that the substitution of A-site cations has some effects on the local chemical environment, bonding distance, and bonding angle of Mn^{2+} ions in the structure. In the structures of $NaMn_3Ca_3S_8$ and CMGS, the A-based (A = Na or Ca) polyhedra are surrounded by Mn–S single chains composed of edge-sharing MnS_6 octahedra (Fig. 5a and b). When the Na^+ cations are replaced by the Ca^{2+} cations, it causes a slight squeeze between the MnS_6 octahedra. As a result, the Mn(3) atoms deviate off the chains extending along the c-axis, which leads to a change in the distances of Mn–Mn between two chains from 6.5144 Å in $NaMn_3Ca_3S_8$ to 6.5642 Å in CMGS. Also, the distance between two Mn atoms in the same chain changes (Fig. 5c and d). Accordingly, the distances of Mn–Mn in the double chains composed of a MnS_6 octahedron also change. Besides, the arrangement mode of Ca^{2+} cations is different from that of Na^+ cations, resulting in a change in the local chemical environment of Mn^{2+}. As such, the increased
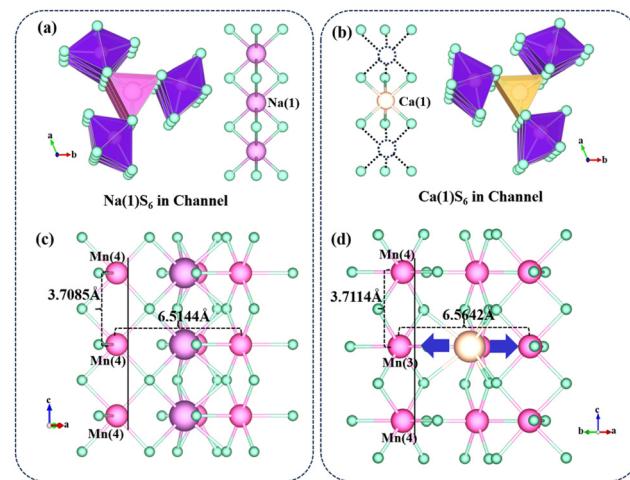
Fig. 5 Distribution of A-site cations in channels of $NaMn_3Ga_3S_8$ and $CaMn_6Ga_6S_{16}$.
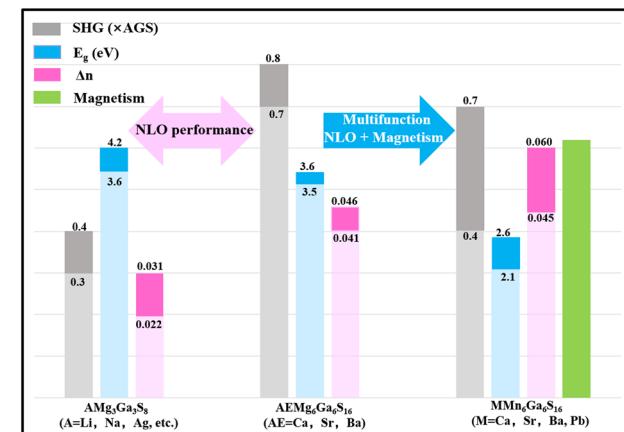
Fig. 6 Performance changes of $A(I)B_3C_3S_8$ and $(AE/M)Mg_6Ga_6S_{16}$ after element substitution.

This journal is © the Partner Organisations 2024

Inorg. Chem. Front., 2024, **11**, 5465–5472 | **5469**

distances of Mn–Mn in two chains and the different local chemical environments around Mn–S single chains caused by the substituted cation may be the reason for the difference in the magnetic properties. During the research process, it was found that the substitution of A- and C-sites in the $A(I)B_3C_3Q_8$ and $AE(II)Mg_6Ga_6Q_{16}$ systems can improve their linear or non-linear optical performances. However, in this study, by replacing their B-sites with Mn atoms, $MMn_6Ga_6S_{16}$ (M = Ca, Sr, Ba, Pb) exhibit not only NLO performances but also paramagnetism (Fig. 6). This indicates that $MMn_6Ga_6S_{16}$ (M = Ca, Sr, Ba, Pb) can serve as potential multifunctional materials.

Conclusions

In summary, four NCS chalcogenides, $MMn_6Ga_6S_{16}$ (M = Ca, Sr, Ba, Pb), were successfully synthesized using the high-temperature sealed-tube method. They all crystallize in the space group $P\bar{6}$ of the hexagonal system, featuring open frameworks built by Mn–S and Ga–S single/double chains, and channels filled with alkaline-earth metal cations. The systematic structural analysis indicates that the low-dimensional structure, i.e. these 1D chains, brings great flexibility and adjustability to different-site substitution in $A(I)B_3C_3Q_8$ and $AE(II)Mg_6Ga_6Q_{16}$. Performance measurement shows that $MMn_6Ga_6S_{16}$ (M = Ca, Sr, Ba, Pb) not only exhibit a wide IR transmission region, suitable SHG response (0.4–0.7 × AGS) and high LIDT (4.8–5.6 × AGS) but also possess the temperature-dependent paramagnetism. Besides, the study of the structure–property relationship indicates that distorted MnS_6 octahedra and GaS_4 tetrahedra and their well-ordered arrangement are responsible for the NLO response of $MMn_6Ga_6S_{16}$ (M = Ca, Sr, Ba, Pb) and structural anisotropy. This work not only provides a wide material platform to explore new IR-NLO chalcogenides by coupling different kinds of chains in one structure but also can improve or enrich material functionality by introducing functional element-based chains.

Author contributions

Writing – original draft: Kaixuan Li, Yujie Zhang and Xianchao Zhu; writing – review and editing: Hongping Wu; resources: Zhanggui Hu; and supervision: Jiyang Wang and Yicheng Wu.

Data availability

1. The data supporting this article have been included as part of the ESI.†
2. Crystallographic data for 2350610–2350613 have been deposited at the CCDC.†

Conflicts of interest

There are no conflicts to declare.

Acknowledgements

References

1 K. Wu, Z. H. Yang and S. L. Pan, The first quaternary diamond-like semiconductor with 10-membered LiS_4 rings exhibiting excellent nonlinear optical performances, *Chem. Commun.*, 2017, **53**, 3010–3013.

2 L. Kang, F. Liang, X. X. Jiang, Z. S. Lin and C. T. Chen, First-Principles Design and Simulations Promote the Development of Nonlinear Optical Crystals, *Acc. Chem. Res.*, 2019, **53**, 209–217.

3 W. L. Yin, A. K. Iyer, C. Li, J. Y. Yao and A. Mar, $Ba_5CdGa_6Se_{15}$, a congruently-melting infrared nonlinear optical material with strong SHG response, *J. Mater. Chem. C*, 2017, **5**, 1057–1063.

4 K. Wu and S. L. Pan, A review on structure-performance relationship toward the optimal design of infrared nonlinear optical materials with balanced performances, *Coord. Chem. Rev.*, 2018, **377**, 191–208.

5 Y. Pan, S. P. Guo, B. W. Liu, H. G. Xue and G. C. Guo, Second-order nonlinear optical crystals with mixed anions, *Coord. Chem. Rev.*, 2018, **374**, 464–496.

6 S. Y. Zhang, D. J. Mei, X. Du, Z. S. Lin, J. B. Zhong, Y. D. Wu and J. L. Xu, The structure and band gap design of high Si doping level $Ag_{1-x}Ga_{1-x}Si_xSe_2$ (x=1/2), *J. Solid State Chem.*, 2016, **238**, 21–24.

7 H. N. Liu, H. P. Wu, Z. G. Hu, J. Y. Wang, Y. C. Wu and H. W. Yu, $Cs_3[(BOP)_2(B_3O_7)_3]$: A Deep-Ultraviolet Nonlinear Optical Crystal Designed by Optimizing Matching of Cation and Anion Groups, *J. Am. Chem. Soc.*, 2023, **145**, 12691–12700.

8 X. Y. Zhang, Y. Q. Liu, M. S. Molokeev, B. H. Xu, X. X. Jiang and Z. S. Lin, Realizing Persistent Zero Area Compressibility over a Wide Pressure Range in Cu_2GeO_4 by Microscopic Orthogonal-Braiding Strategy, *Angew. Chem., Int. Ed.*, 2023, **63**, e202318401.

9 H. P. Wu, S. L. Pan, K. R. Poeppelmeier, H. Y. Li, D. Z. Jia, Z. H. Chen, X. Y. Fan, Y. Yang, J. M. Rondinelli and H. S. Luo, $K_3B_6O_{10}Cl$: A New Structure Analogous to Perovskite with a Large Second Harmonic Generation Response and Deep UV Absorption Edge, *J. Am. Chem. Soc.*, 2011, **133**, 7786–7790.

10 B. B. Zhang, G. Q. Shi, Z. H. Yang, F. F. Zhang and S. L. Pan, Fluorooxoborates: Beryllium-Free Deep-Ultraviolet Nonlinear Optical Materials without Layered Growth, *Angew. Chem., Int. Ed.*, 2017, **56**, 3916–3919.

11 M. Mutailipu, M. Zhang, B. B. Zhang, L. Y. Wang, Z. H. Yang, X. Zhou and S. L. Pan, $SrB_5O_7F_3$ Functionalized with $[B_5O_9F_3]^{6-}$ Chromophores: Accelerating the Rational

Design of Deep-Ultraviolet Nonlinear Optical Materials, *Angew. Chem., Int. Ed.*, 2018, **57**, 6095–6099.

12 Y. Wang, B. B. Zhang, Z. H. Yang and S. L. Pan, Cation-Tuned Synthesis of Fluorooxoborates: Towards Optimal Deep-Ultraviolet Nonlinear Optical Materials, *Angew. Chem., Int. Ed.*, 2018, **57**, 2150–2154.

13 J. H. Zhang, D. J. Clark, J. A. Brant, K. A. Rosmus, P. Grima, J. W. Lekse, J. I. Jang and J. A. Aitken, α-Li_2ZnGeS_4: A Wide-Bandgap Diamond-like Semiconductor with Excellent Balance between Laser-Induced Damage Threshold and Second Harmonic Generation Response, *Chem. Mater.*, 2020, **32**, 8947–8955.

14 J. P. Yohannan and K. Vidyasagar, Syntheses and structural characterization of non-centrosymmetric $Na_2M_2M'S_6$ (M, M'=Ga, In, Si, Ge, Sn, Zn, Cd) sulfides, *J. Solid State Chem.*, 2016, **238**, 147–155.

15 A. Abudurusuli, J. B. Huang, P. Wang, Z. H. Yang, S. L. Pan and J. J. Li, $Li_4MgGe_2S_7$: The First Alkali and Alkaline-Earth Diamond-Like Infrared Nonlinear Optical Material with Exceptional Large Band Gap, *Angew. Chem., Int. Ed.*, 2021, **60**, 24131–24136.

16 X. Y. Zhang, H. P. Wu, Z. G. Hu, J. Y. Wang, Y. C. Wu and H. W. Yu, $A^{II}HgMIVS_4$ (A^{II} = Sr, Ba, MIV = Si, Ge): A Series of Materials with Large Second Harmonic Generation Response and Wide Band Gaps, *Adv. Opt. Mater.*, 2023, **12**, 2301735.

17 M. Mutailipu, Z. Li, M. Zhang, D. W. Hou, Z. H. Yang, B. B. Zhang, H. P. Wu and S. L. Pan, The mechanism of large second harmonic generation enhancement activated by Zn (2+) substitution, *Chem. Phys.*, 2016, **18**, 32931–32936.

18 S. B. Mirova, A. O. Okorogu, W. Lee, D. I. Crouthamel, N. Jenkins, A. Yu. Dergachev, K. L. Vodopyanov and V. V. Badikov, Tunable middle infrared downconversion in GaSe and $AgGaS_2$, *Opt. Commun.*, 1998, **155**, 307–312.

19 L. R. Shiozawa, G. C. Catella, J. R. Hietanen, R. C. Eckardt, R. K. Route, R. S. Feigelson, D. G. Cooper and C. L. Marquardt, Mid-IR absorption in $AgGaSe_2$ optical parametric oscillator crystals, *Appl. Opt.*, 1993, **32**, 3948–3951.

20 F. Rotermund, V. Petrov and F. Noack, Schunemann, Femtosecond parametric generation in $ZnGeP_2$, *Opt. Lett.*, 1999, **24**, 414–416.

21 Z. G. Xia and K. R. Poeppelmeier, Chemistry-Inspired Adaptable Framework Structures, *Acc. Chem. Res.*, 2017, **50**, 1222–1230.

22 K. X. Ding, H. P. Wu, Z. G. Hu, J. Y. Wang, Y. C. Wu and H. W. Yu, $[Ba_4(S_2)][ZnGa_4S_{10}]$: Design of an Unprecedented Infrared Nonlinear Salt-Inclusion Chalcogenide with Disulfide-Bonds, *Small*, 2023, **19**, 2302819.

23 Y. J. Zhang, Q. Bian, H. P. Wu, H. W. Yu, Z. G. Hu, J. Y. Wang and Y. C. Wu, Designing A New Infrared Nonlinear Optical Material, β-$BaGa_2Se_4$ Inspired by the Phase Transition of the BaB_2O_4 (BBO) Crystal, *Angew. Chem., Int. Ed.*, 2021, **61**, e202115374.

24 Z. Qian, Q. Bian, H. P. Wu, H. W. Yu, Z. S. Lin, Z. G. Hu, J. Y. Wang and Y. C. Wu, β-$BaGa_4Se_7$: a promising IR non-

linear optical crystal designed by predictable structural rearrangement, *J. Mater. Chem. C*, 2022, **10**, 96–101.

25 Y. S. Cheng, H. P. Wu, H. W. Yu, Z. G. Hu, J. Y. Wang and Y. C. Wu, Rational design of a promising oxychalcogenide infrared nonlinear optical crystal, *Chem. Sci.*, 2022, **13**, 5305–5310.

26 R. Q. Wang, F. Liang, X. Liu, Y. Xiao, Q. Q. Liu, X. Zhang, L. M. Wu, L. Chen and F. Q. Huang, Heteroanionic Melilite Oxysulfide: A Promising Infrared Nonlinear Optical Candidate with a Strong Second-Harmonic Generation Response, Sufficient Birefringence, and Wide Bandgap, *ACS Appl. Mater. Interfaces*, 2022, **14**, 23645–23652.

27 T. Endo, Y. Doi, M. Wakeshima, K. Suzuki, Y. Matsuo, K. Tezuka, T. Ohtsuki, Y. J. Shan and Y. Hinatsu, Magnetic Properties of the Melilite-Type Oxysulfide $Sr_2MnGe_2S_6O$: Magnetic Interactions Enhanced by Anion Substitution, *Inorg. Chem.*, 2017, **56**, 2459–2466.

28 S. M. Pei, B. W. Liu, W. F. Chen, X. M. Jiang and G. C. Guo, Breaking the bottleneck of simultaneously wide band gap and large nonlinear optical coefficient by a "pore recon-struction" strategy in a salt-inclusion chalcogenide, *Mater. Horiz.*, 2023, **10**, 2921–2926.

29 B. W. Liu, S. M. Pei, X. M. Jiang and G. C. Guo, Broad trans-parency and wide band gap achieved in a magnetic infrared nonlinear optical chalcogenide by suppressing d-d tran-sitions, *Mater. Horiz.*, 2022, **9**, 1513–1517.

30 R. Q. Wang, X. Zhang and F. Q. Huang, $[Cs_6Cl][Ga_5GeQ_{12}]$ (Q = S, Se): two novel porous layered chalcohalides exhibit-ing two-band emission and ion exchange properties, *Sci. China: Chem.*, 2022, **65**, 1903–1910.

31 Y. F. Song, S. X. Cui, Z. Qian, H. W. Yu, Z. G. Hu, J. Y. Wang, Y. C. Wu and H. P. Wu, $[ASr_4Cl][Ge_3S_{10}]$ (A = Na, K) and $[KBa_4Cl][Ge_3S_{10}]$: new salt-inclusion infrared non-linear optical crystals with zero-dimensional $[Ge_3S_9]$ clus-ters, *Inorg. Chem. Front.*, 2022, **9**, 5932–5940.

32 S. X. Cui, H. P. Wu, Z. G. Hu, J. Y. Wang, Y. C. Wu and H. W. Yu, The Antiperovskite-Type Oxychalcogenides Ae_3Q $[GeOQ_3]$ (Ae = Ba, Sr; Q = S, Se) with Large Second Harmonic Generation Responses and Wide Band Gaps, *Adv. Sci.*, 2022, **10**, 2204755–2204755.

33 L. Luo, L. N. Wang, J. B. Chen, J. Z. Zhou, Z. H. Yang, S. L. Pan and J. J. Li, $A^IB_3^{II}C_3^{III}Q_8^{VI}$: A New Family for the Design of Infrared Nonlinear Optical Materials by Coupling Octahedra and Tetrahedra Units, *J. Am. Chem. Soc.*, 2022, **144**, 21916–21925.

34 J. L. Chen, Y. J. Zhang, H. P. Wu, Z. G. Hu, J. Y. Wang, Y. C. Wu and H. W. Yu, $AeMg_6Ga_6S_{16}$ (Ae = Ca, Sr, Ba): The First Double Alkaline-Earth Metal Chalcogenides with Excellent Performances, *Adv. Opt. Mater.*, 2022, **11**, 2202147.

35 L. N. Wang, D. D. Chu, Z. H. Yang, J. J. Li and S. L. Pan, Wide band gap selenide infrared nonlinear optical materials $A^{II}Mg_6Ga_6Se_{16}$ with strong SHG responses and high laser-induced damage thresholds, *Chem. Sci.*, 2024, **15**, 6577–6582.

36 Y. J. Zhang, J. L. Chen, K. X. Li, H. P. Wu, Z. G. Hu, J. Y. Wang, Y. C. Wu and H. W. Yu, $LaMg_6Ga_6S_{16}$: a chemi-

cal stable divalent lanthanide chalcogenide, *Nat. Commun.*, 2024, **15**, 2959.

37 P. C. Yang, H. P. Wu, Z. G. Hu, J. Y. Wang, Y. C. Wu and H. W. Yu, $NaMn_3Ga_3S_8$: Noncentrosymmetric inorganic metal chalcogenide with nonlinear optical response, antiferromagnetic, and photoluminescence performances, *Mater. Today Chem.*, 2023, **33**, 101727.

38 J. X. Zhang, P. Feng, M. Y. Ran, X. T. Wu, H. Lin and Q. L. Zhu, Ga-based IR nonlinear optical materials: Synthesis, structures, and properties, *Coord. Chem. Rev.*, 2024, **502**, 215617.

39 D. Altermatt and I. D. Brown, Bond-Valence Parameters Obtained from a Systematic Analysis of the Inorganic Crystal Structure Database, *Acta Crystallogr., Sect. B: Struct. Sci.*, 1985, **41**, 244–247.

40 K. Wu, Z. H. Yang and S. L. Pan, Na_2BaMQ_4 (M=Ge, Sn; Q=S, Se): Infrared Nonlinear Optical Materials with Excellent Performances and that Undergo Structural Transformations, *Angew. Chem., Int. Ed.*, 2016, **55**, 6713–6715.

41 S. Liu, X. M. Liu, S. G. Zhao, Y. C. Liu, L. N. Li, Q. R. Ding, Y. Q. Li, Z. S. Lin, J. H. Luo and M. C. Hong, An Exceptional Peroxide Birefringent Material Resulting from d–π Interactions, *Angew. Chem., Int. Ed.*, 2020, **59**, 9414–9417.

42 Y. Zhang, L. Wu, Y. F. Kong, T. Q. Sun, J. J. Xu and X. L. Chen, Structure Determination of Novel Orthoborate $NaMgBO_3$: A Promising Birefringent Crystal, *Inorg. Chem.*, 2007, **46**, 5207–5211.

43 M. M. Chen, S. H. Zhou, W. B. Wei, X. T. Wu, H. Lin and Q. L. Zhu, Phase Matchability Transformation in the Infrared Nonlinear Optical Materials with Diamond-Like Frameworks, *Adv. Opt. Mater.*, 2021, **10**, 2102123.

44 S. K. Kurtz and T. T. Perry, A Powder Technique for the Evaluation of Nonlinear Optical Materials, *J. Appl. Phys.*, 1968, **39**, 3798–3813.

45 N. Rodier, M. Guittard and J. Flahaut, Structure cristalline de $La_6Mn_2Ga_2S_{14}$, *C. R. Seances Acad. Sci.*, 1983, **296**, 65.

46 J. Leal-Gonzalez, S. S. Melibary and A. J. Smith, Structure of Lithium Gallium Sulfide, $LiGaS_2$, *Acta Crystallogr.*, 1990, **46**, 2017.

47 Z. Qian, H. N. Liu, Y. J. Zhang, H. P. Wu, Z. G. Hu, J. Y. Wang, Y. C. Wu and H. W. Yu, The exploration of new infrared nonlinear optical crystals based on the polymorphism of $BaGa_4S_7$, *Inorg. Chem. Front.*, 2022, **9**, 4632–4641.

48 Z. Li, X. X. Jiang, C. J. Yi, M. L. Zhou, Y. W. Guo, X. Y. Luo, Z. S. Lin, Y. C. Wu, Y. G. Shi and J. Y. Yao, $K_2MnGe_3S_8$: a new multifunctional semiconductor featuring $[MnGe_3S_8]^{2-}$ layers and demonstrating interesting nonlinear optical response and antiferromagnetic properties, *J. Mater. Chem. C*, 2018, **6**, 10042–10049.

49 Z. Z. Luo, C. S. Lin, W. D. Cheng, Y. B. Li, H. Zhang, W. L. Zhang and Z. Z. He, Syntheses and characterizations of compounds $Ba_4F_4XGa_2S_6$ (X = Cr, Mn, Fe) and $Ba_4F_4MnIn_2S_6$ with 2D layered structures, *Dalton Trans.*, 2013, **42**, 9938–9945.

50 G. H. Wang, C. Y. Xu, H. B. Cao, T. Hong, Q. Huang, Q. Y. Ren, J. Q. Xu, H. D. Zhou, W. Luo, D. Qian and J. Ma, Magnetic properties of the low-dimensional $BaM_2Si_2O_7$ system (M=Cu, Co, Mn), *Phys. Rev. B*, 2019, **100**, 035131.

51 S. B. Karki and F. Ramezanipour, Magnetic and electrical properties of $BaSrMMoO_6$ (M = Mn, Fe, Co, and Ni), *Mater. Today Chem.*, 2019, **13**, 25–33.

52 C. J. O'connor, Magnetochemistry-Advances in Theory and Experimentation, *Prog. Inorg. Chem.*, 1982, **29**, 203–283.

5472 | *Inorg. Chem. Front.*, 2024, **11**, 5465–5472

This journal is © the Partner Organisations 2024